Ground Vehicle Spectral and Polarization Imaging Sensor

Corrie Vandervlugt[a], Robert Sampson[b], Robert Karlsen[c]
a: College of Optical Sciences, University of Arizona, Tucson, AZ 85721
b: I Technology Applications, Ann Arbor, MI 48103
c: U.S. Army TACOM, Warren, MI 48397

ABSTRACT

This paper summarizes the design of an Imaging Spectropolarimeter that operates in the visible wavelength region. The sensor uses computed tomographic imaging techniques to instantaneously form an object cube (spectral and spatial image) during each frame time. This computed tomographic imaging spectrometer (CTIS) is then combined with a channeled spectropolarimeter (CHSP) to form a computed tomography imaging channeled spectropolarimeter (CTICS)) which can simultaneously obtain image spatial and spectral information as well as polarization Stokes vectors at each resolution element in a single focal plane array (FPA) integration time with no moving parts. The work described in this paper is being performed by I Technology Applications and The University of Arizona Optical Sciences Center. Calibration techniques as well as reconstruction investigations are discussed. Spectral and polarization measurement results are described. The applications of the sensor include target detection and recognition as well as navigation and environmental monitoring.

INTRODUCTION

A Computed Tomography Imaging Spectrometer (CTIS) is an imaging spectrometer which can obtain full spatial and spectral (x, y, λ) information from a scene in a single integration time with no moving parts. Other conventional imaging spectrometers, such as whiskbroom or pushbroom spectrometers, require scanning to obtain a full data cube. CTIS acquires the data cube by using limited angle computed tomography techniques in complex post-processing algorithms to reconstruct the image cube from its 2-D projections formed on the focal plane array (FPA).[1]

The CTIS design, shown in Figure 1, uses an objective lens to focus the image of a scene onto an intermediate image plane. A field stop is placed at this plane to limit the spatial extent of the object. Light from the intermediate image is collimated and sent through a 2-D dispersing (grating) element and then refocused onto the FPA. The computer generated hologram (CGH) disperser is the element that is responsible for forming the array of spectrally dispersed, 2-D projections from the 3-D object cube (see Figure 2).[2] The most common CGH design used makes a grid of 5x5 diffraction orders in the focal plane (see Figure 2).

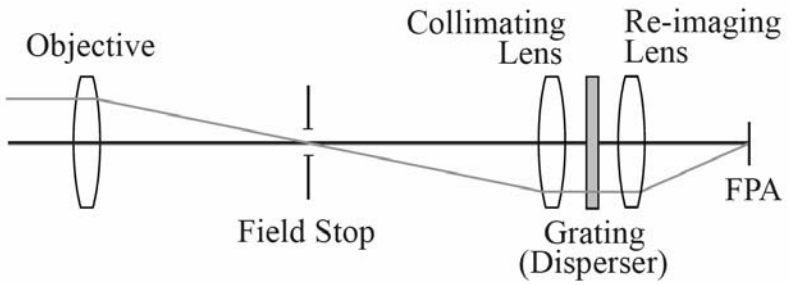

Figure 1: schematic layout of the CTIS

Report Documentation Page

Form Approved
OMB No. 0704-0188

1. REPORT DATE	2. REPORT TYPE	3. DATES COVERED
30 OCT 2007	**N/A**	

4. TITLE AND SUBTITLE	5a. CONTRACT NUMBER
Ground Vehicle Spectral and Polarization Imaging Sensor	5b. GRANT NUMBER
	5c. PROGRAM ELEMENT NUMBER
6. AUTHOR(S)	5d. PROJECT NUMBER
; ; Vandervlugt /CorrieSampson /RobertKarlsen /Robert	5e. TASK NUMBER
	5f. WORK UNIT NUMBER
7. PERFORMING ORGANIZATION NAME(S) AND ADDRESS(ES)	8. PERFORMING ORGANIZATION REPORT NUMBER
US Army RDECOM-TARDEC 6501 E 11 Mile Rd Warren, MI 48397-5000	**18370**
9. SPONSORING/MONITORING AGENCY NAME(S) AND ADDRESS(ES)	10. SPONSOR/MONITOR'S ACRONYM(S)
TACOM TARDEC	11. SPONSOR/MONITOR'S REPORT NUMBER(S)

12. DISTRIBUTION/AVAILABILITY STATEMENT

Approved for public release, distribution unlimited.

13. SUPPLEMENTARY NOTES

The original document contains color images.

14. ABSTRACT

15. SUBJECT TERMS

16. SECURITY CLASSIFICATION OF:			17. LIMITATION OF ABSTRACT	18. NUMBER OF PAGES	19a. NAME OF RESPONSIBLE PERSON
a. REPORT	b. ABSTRACT	c. THIS PAGE			
unclassified	**unclassified**	**unclassified**	**SAR**	**14**	

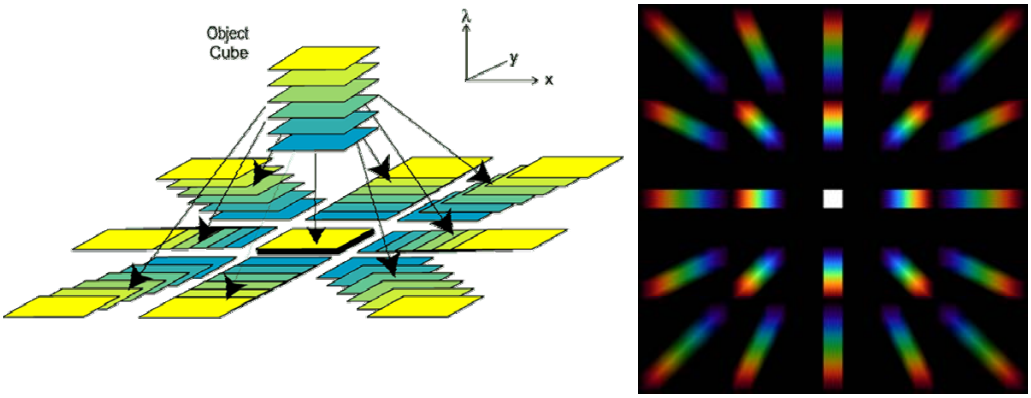

Figure 2: (Left) Sketch showing spectrally dispersed 2-D projections from the 3-D object cube; (Right) 5x5 CGH diffraction pattern

This paper describes the development of a visible imaging sensor that provides spatial, spectral, and polarimetric data sets simultaneously. The basic system operates with no moving parts and is ideal for problems involving the need for real time spatial, spectral, and polarization information. The sensor is designed to provide spatial, spectral and polarization data sets every frame time for detection, discrimination and navigation for robotic vehicle applications. The spectro-polarimeter involves the unique combination of channeled spectro-polarimetry with computed tomographic imaging spectrometry (CTIS). Channeled spectro-polarimetry uses modulation to encode the spectral dependence of the Stokes parameters in a single spectrum. The combination of these techniques provides the basis for an imaging Stokes spectro-polarimeter that can be implemented with no moving parts.

Channeled spectropolarimetry is a technique in which the simple addition of a pair of thick, high order retarders and an analyzer to an optical system enables the conversion of a spectrometer into a spectropolarimeter. Figure 3 illustrates the configuration of a channeled spectropolarimeter (CHSP). The input broadband spectrum passes through two high-order retarders, the first of which is aligned with the analyzer's transmission axis, and the second is aligned at 45º to the first. An unpolarized input will reach the spectrometer essentially unmodified, whereas a polarized input will be modulated at high frequencies, due to the orientation of the retarders and analyzer. The frequency of the modulation carries information about the distribution of the Stokes components across the spectrum.[3,4] Using Mueller calculus, and representing the spectrum in terms of wave number, σ, we can relate the measured spectrum I(σ) in terms of the Stokes vector polarization components in the input beam

$$2I(\sigma) = S_0 + S_1\cos(\delta_2) + S_2\sin(\delta_1)\sin(\delta_2) - S_3\cos(\delta_1)\sin(\delta_2) \tag{1}$$

where δ_1 and δ_2 are the retardances of the respective retarders (and each are linear functions of wavenumber, σ). Taking the Fourier transform of I(σ), we obtain a function in which the four individual Stokes components are separated into seven channels (the seven terms of the above equation). By proper choice of thicknesses for the two retarders, which determine the retardances, δ_1 and δ_2, these channels do not overlap, so that by windowing each channel individually and taking the forward Fourier transform of the result, we obtain the four spectrally-resolved Stokes components.

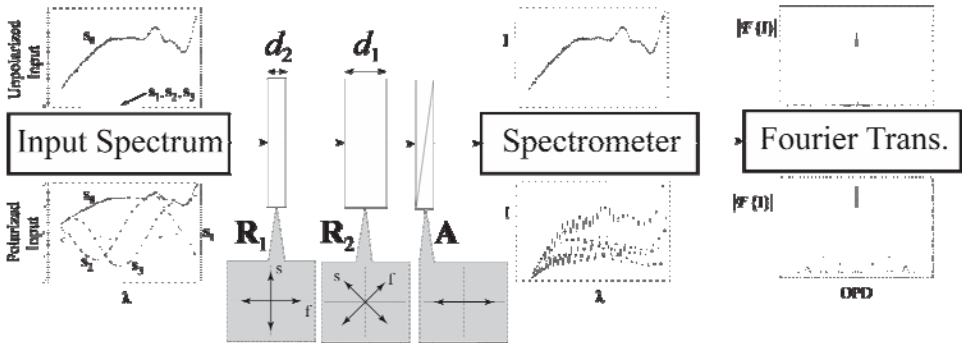

Figure 3: Schematic diagram of a channeled spectropolarimeter.

By combining the techniques of CTIS with channeled spectropolarimetry, an instrument is constructed which maintains snapshot capability and obtains information for the four-dimensional hypercube (spatial, spectral, and polarimetric information). Fusing the two techniques involves the insertion of the pair of high-order retarders and analyzer into the collimated path in front of the CTIS disperser, so that the polarization information in the measured scene can now be encoded in modulations of the spectrum. Figure 4 (right) shows the schematic diagram of the CTIS combined with the channeled spectropolarimeter. The combined instrument is called a computed tomography imaging channeled spectropolarimeter (CTICS). Figure 4 also shows an example of how a CTIS image looks with a modulated spectrum. This additional capability comes at the cost of reducing the spectral resolution by a factor of 7, but snapshot capability is maintained.

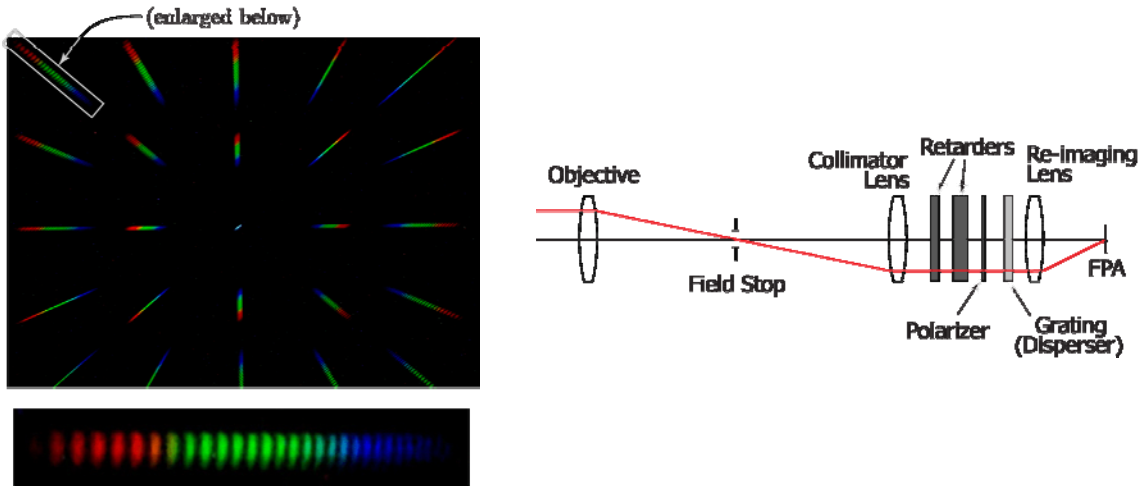

Figure 4: (Left) Image of horizontally-polarized light through a narrow slit. (Right) The layout of the CTICS system, with the pair of high-order retarders and analyzer inserted in front of the disperser.

VISIBLE CTICS DESIGN

The CTICS instrument built for this research was made to work in the visible (420 – 700nm) spectral region. A 4-megapixel industrial camera is used with standard Nikon zoom lenses. The CGH disperser employs the 5x5 diffraction pattern design etched onto PMMA plastic. The two retarders are made out of quartz and are AR coated for the visible spectrum. Their thicknesses are 1.31mm and 2.62mm. The thicknesses for the retarders were determined using known instrument parameters and our CTICS computer simulator. The analyzer is a standard sheet polarizer. An image of the instrument is shown in Figure 5.

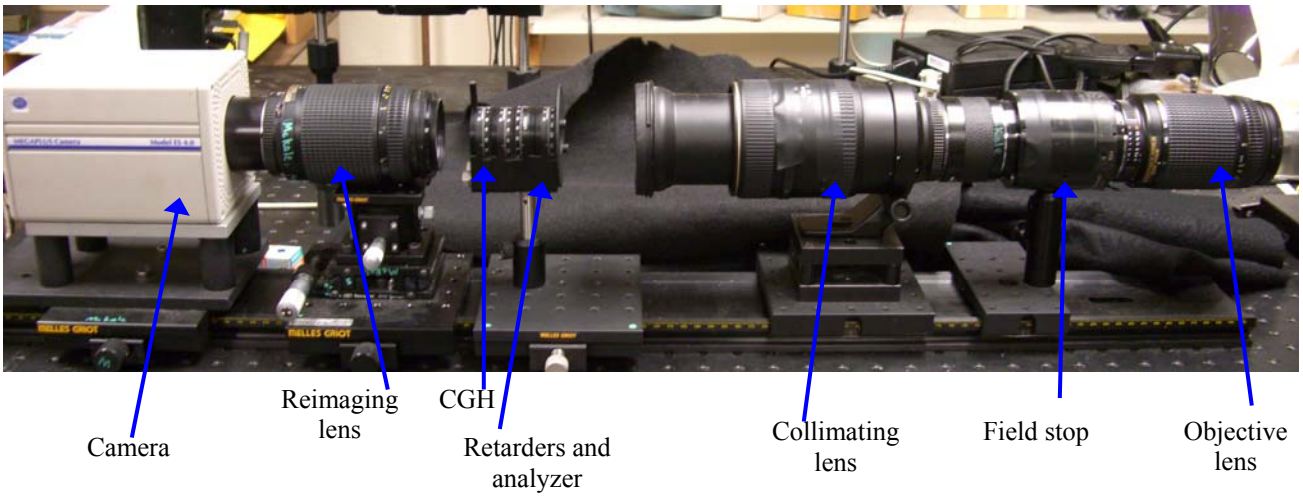

Figure 5: picture of CTICS instrument with labels showing individual elements

CALIBRATION AND OBJECT CUBE RECONSTRUCTION

Calibration for the CTIS system involves the setup of a special calibration system consisting of a tungsten-halogen light source, a monochromator, fiber optic waveguide, and a calibrated radiometer. The halogen lamp illumination system is coupled into the entrance slit of a monochromator. A narrow wavelength band is selected by the monochromator and imaged into the fiber optic waveguide through the exit slit. The other end of the waveguide is butted directly into the field stop of the CTIS (Figure 6)

Figure 6: Mirror and fiber optic waveguide at exit slit of monochromator

The calibration process is as follows. First, we attached the source to the input face of the monochromator. Then, light from the exit slit of the monochromator must be coupled into the fiber optic waveguide. This is done by mounting the fiber on a translation stage that has 3 degrees of movement (x,y,z) and using a mirror to focus the light down onto the fiber. A photo showing the light exiting the monochromator being coupled into the fiber is shown in Figure 6. In order to insure the fiber was getting the maximum possible light coupled into it, the other end of the waveguide was hooked into a spectrometer that showed signal level. The x, y, z translation stages were adjusted until the spectrometer was receiving a maximum signal. Then, this end of the waveguide was mounted in front of a calibrated UDT radiometer in order to measure the intensity at each wavelength. This data was saved as a text file and is used by the calibration software.

Next, the whole field stop was illiminated with a tungsten-halogen source, so the coordinates of the central order could easily be determined. These coordinates were hard coded into the calibration software. Once the coordinates of the zero order were known, the calibration program draws a red box on the screen to show the zero order's location. This was used when aligning the fiber optic waveguide into the center of the field stop. The end of the waveguide that is placed at the center of the field stop was also mounted on three translation stages. The location of the fiber was adjusted until it was in the center of the newly defined zero order. The next component added to the system was a band-pass filter to make sure wavelengths that are not in the spectrum of interest do not get into the system. This is necessary to prevent overlap in some of the orders as well. A typical image is shown in Figure 7.

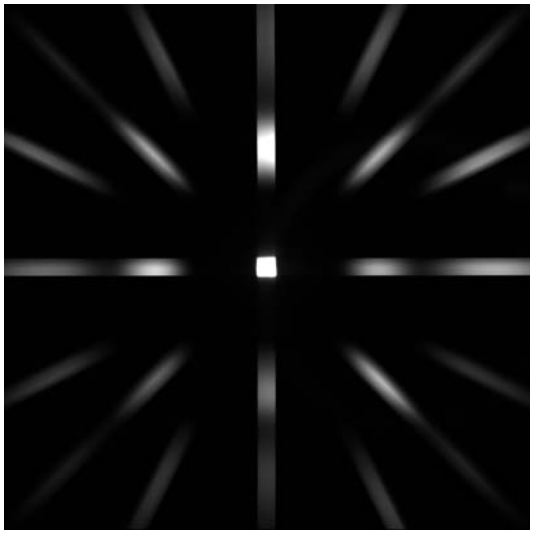

Figure 7: CTIS image with tungsten-halogen lamp illumination

The CTICS system calibration is the same as used for the CTIS with the addition of a known polarization component. A high watt tungsten halogen light bulb is again used as the source. The light is sent through a monochromator and the exiting light from the monochromator is coupled into a 50μm fiber optic waveguide. The fiber is mounted on three translation stages at each end so that it can be adjusted with three different degrees of freedom. In order to make sure the most amount of light is coupled into the fiber, an Ocean Optics spectrometer was used to measure the output intensity of light through the fiber. We started with a very large diameter fiber (400μm) and adjusted the translation stages to get the maximum output. From there, we switched to a smaller fiber (200μm) and readjusted. We did this again with a 100μm fiber and finally with a 50μm fiber.

The other end of the fiber optic waveguide is mounted and positioned so that it is in the center of the field stop. Before placing the fiber into the field stop a white light lamp was used to check the size and location of the field stop. We found

that the location of the field stop, after some adjustments were made to the instrument, had shifted a few pixels. We hard coded the change of the location and size of the field stop. After this was completed, the fiber was positioned in the center of the field stop.

After calibrating the instrument, data was taken using a 400μm fiber optic waveguide with an Ocean Optics broadband source. This effectively makes a broadband distant point object. A filter was used with the source to limit the intensity in the red end of the spectrum. An intensity profile of the unpolarized source with the filter was measured using an Ocean Optics spectrometer and is shown below in Figure 8. First, images were taken using unpolarized light from the fiber. Then, in order to generate different polarization states, a linear sheet polarizer was set up in front of the CTICS objective lens and rotated to various polarization orientations. Data was taken for horizontally polarized light (positive S_1), 45° polarized light (positive S_2), and vertically polarized light (negative S_1). Reference data was taken with 22.5° polarized light to calibrate the polarimeter.

Reconstruction of the data is based on the Linear Operator Model

$$g = H \cdot f(x, y, \lambda) \tag{2}$$

where f is the object input, g is the image output, and H is the system matrix obtained from calibration. Since the system matrix, H, is very large, calculating a pseudoinverse is not computationally practical using current resources. Instead, iterative reconstruction algorithms are employed. The data in this paper was reconstructed using the Expectation Maximization (EM) iterative algorithm[5]

$$EM: \hat{f}_n^{(k+1)} = \frac{\hat{f}_n^{(k)}}{\sum_{m'=1}^{M} H_{m'n}} \sum_{m=1}^{M} H_{mn}^{\mathrm{T}} \frac{g_m}{\left(H\hat{f}^{(k)}\right)_m} \tag{3}$$

where $\hat{f}$ indicates an estimate of the object's datacube.

Other reconstruction algorithms that dramatically speed up the reconstruction process have been developed and are being tested.

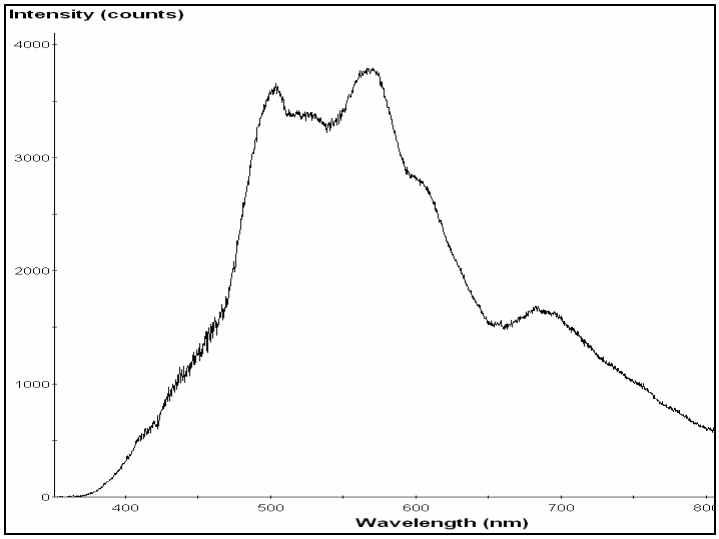

Figure 8: intensity profile of unpolarized broadband source with filter

SPECTRAL AND POLARIZATION RESULTS

Spectral and polarization data collected with the instrument are presented in this collection. These data are a comparable to initial results from one location in the center of the field presented in reference 6.

1. Reconstructions of broadband point source at edge of field

The results of the reconstruction of the unpolarized broadband point source at the edge of the field of view (FOV) are shown in Figure 9a-d. The data from the edge of the field can be compared to previous results of a broadband point source centered in the field to gauge the performance of the CTICS instrument at varying field positions. Figure 9a is the zero order of the raw data and can be compared to the panchromatic image of the data cube in Figure 9b. The spread in the datacube image is partially due to summing up all the individual wavelength bands in the datacube into one, 2-D panchromatic image. The faint gray lines that can be seen in the data cube are ghost artifacts from back-projections in the reconstruction algorithms. Figure 9c shows the reconstructed spectrum of a single spatial position of the datacube in terms of decreasing wavenumber. Since the source is unpolarized, there are no modulations in the reconstructed spectrum. The normalized reconstructed Stokes spectrum for the unpolarized point object is shown in Figure 9d. S_1, S_2, and S_3 should all be zero for unpolarized light. In the plots of the reconstructed Stokes spectra, S_1 is a solid line, S_2 is a dashed line, and S_3 is a dotted line.

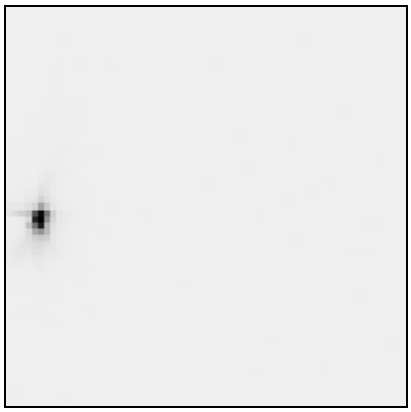

Figure 9a: zero order of raw data

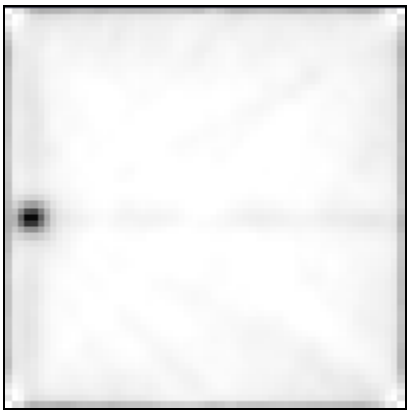

Figure 9b: panchromatic image of data cube

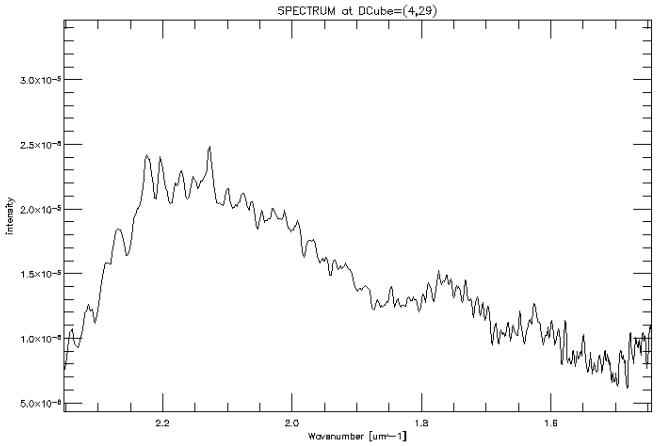

Figure 9c: reconstructed spectrum (wavenumber)

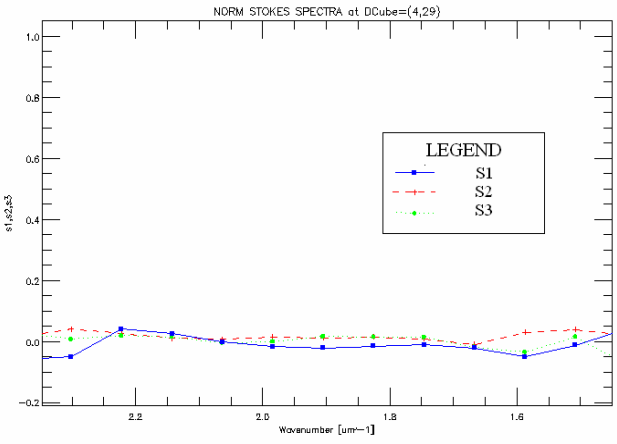

Figure 9d: normalized reconstructed Stokes spectra

The resulting reconstructed spectra and Stokes spectra for the horizontally polarized, vertically polarized, and 45° polarized objects are shown below. The zero order of the raw data and panchromatic image of the datacube for each of the polarized objects look similar to the images in Figures 9a and 9b, respectively; to avoid redundancy, they will not be

repeated here. Figures 10a, 11a, and 12a show the reconstructed spectra for the various polarized objects. The modulations in the spectrum due to the polarization are clearly depicted. Note the modulations for the horizontally polarized object is out of phase with the vertically polarized object, as expected. Figures 10b, 11b, and 12b show the normalized reconstructed Stokes spectra for the various polarized objects. For horizontal polarization, S_1 should be equal to +1 the other two Stokes vectors should be zero. For vertical polarization, S_1 should equal -1 and again the other Stokes vectors should be zero. In the case of 45° polarization, S_2 should equal +1 and the other vectors should be zero.

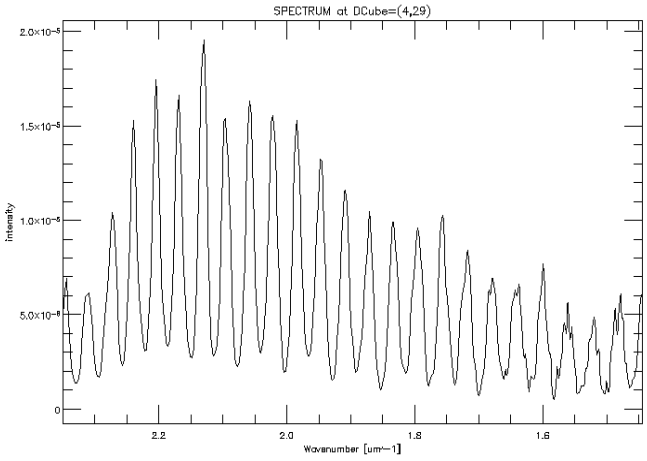

Figure 10a: reconstructed spectrum (wavenumber)

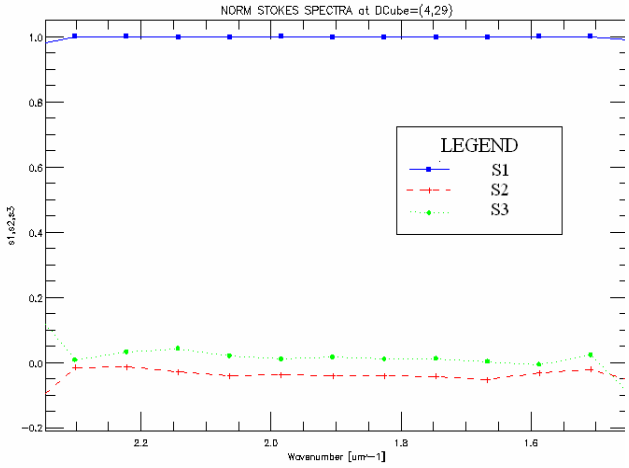

Figure 10b: normalized reconstructed Stokes spectra

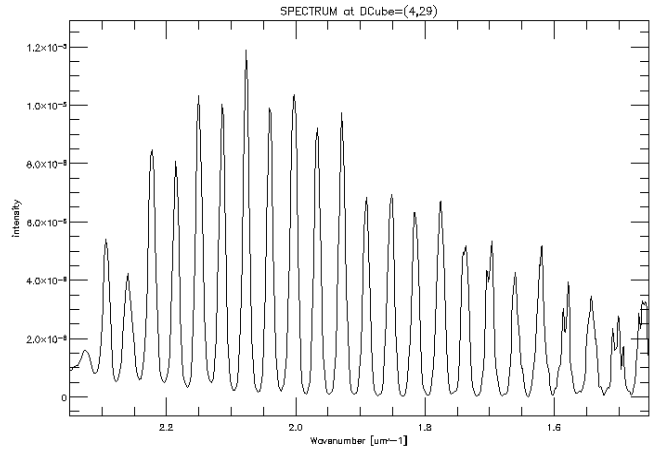

Figure 11a: reconstructed spectrum (wavenumber)

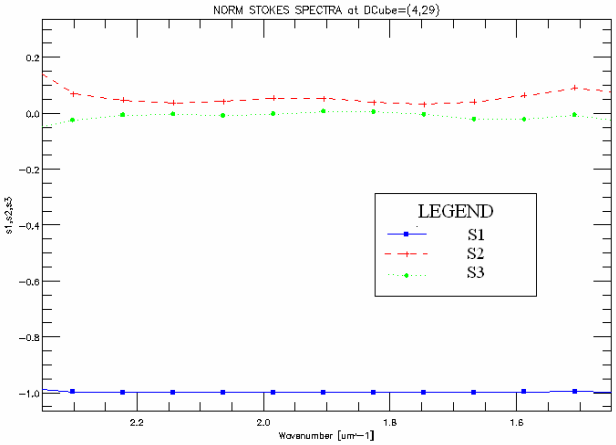

Figure 11b: normalized reconstructed Stokes spectra

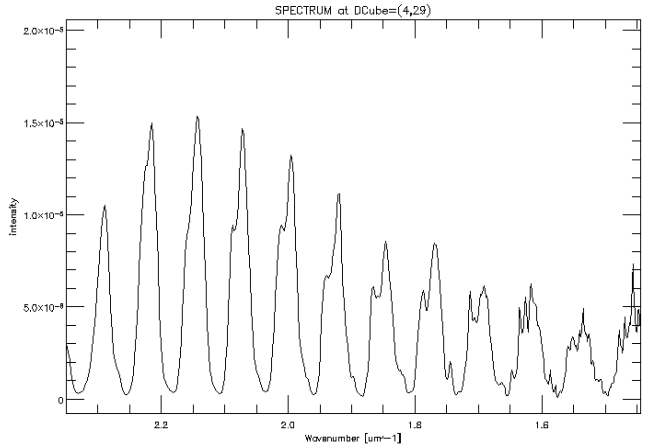

Figure 12a: reconstructed spectrum (wavenumber)

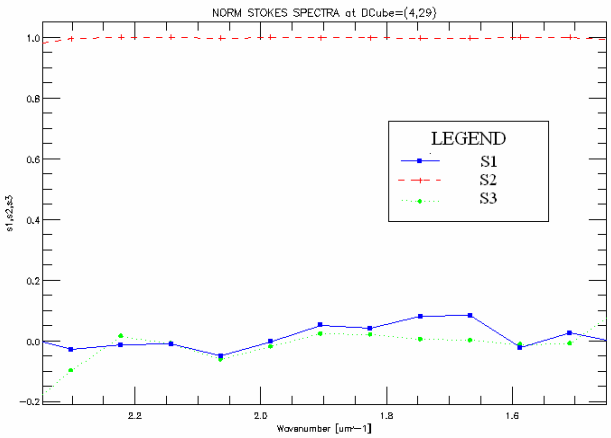

Figure 12b: normalized reconstructed Stokes spectra

2. Reconstructions of polarized LEDs

Polarization data was also taken using the 3-LED (red, green, blue) setup that has been used with the CTIS previously to test spectral reconstructions. The results of the reconstructions are shown in the figures below. Figure 13a,b show the zero order of the raw data and the panchromatic image of the data cube, respectively. The three spots correspond to the 3 LEDs: blue on the left, green in the center, and red on the right. These images look the same for all of the different polarization states, so they will only be shown once. Stokes vectors were analyzed for the blue and green LEDs. The red LED is not spectrally broad enough to achieve a modulated spectrum.

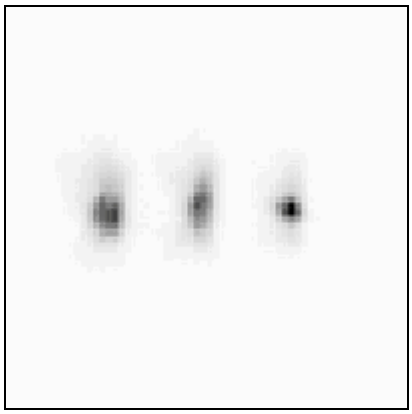

Figure 13a: zero order of raw data

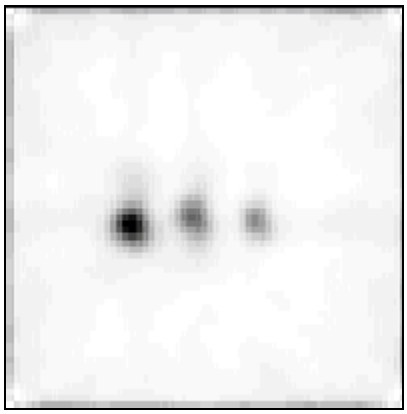

Figure 13b: panchromatic image of data cube

For conciseness only the reconstructed Stokes spectra are shown for the LEDs. Figures 14a and 14b below show the reconstructed Stokes spectra for the horizontally polarized green and blue LEDs, respectively. Figures 15a and 15b show vertically polarized green and blue LEDs, respectively, and Figures 16a and 16b show the reconstructed Stokes spectra for 45° polarized green and blue LEDs.

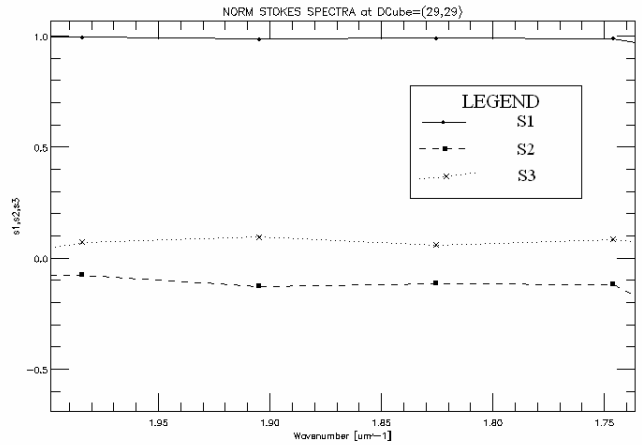

Figure14a: normalized reconstructed Stokes spectra, horizontal polarization (green)

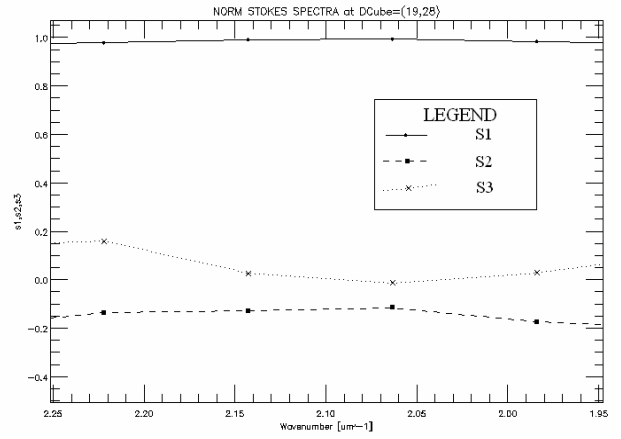

Figure 14b: normalized reconstructed Stokes spectra, horizontal polarization (blue)

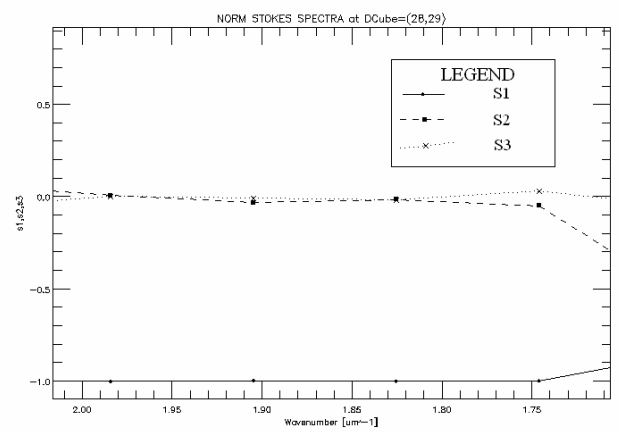

Figure 15a: normalized reconstructed Stokes spectra, vertical polarization (green)

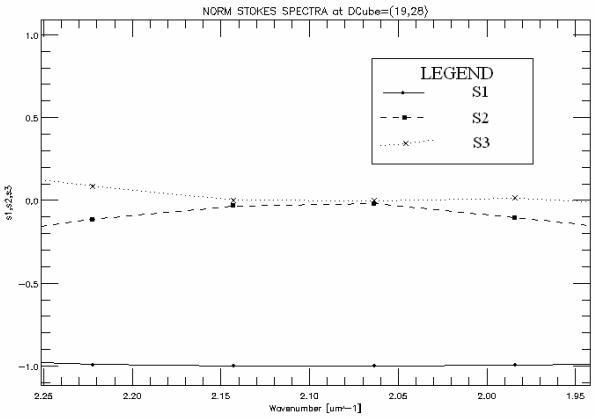

Figure 15b: normalized reconstructed Stokes spectra, vertical polarization (blue)

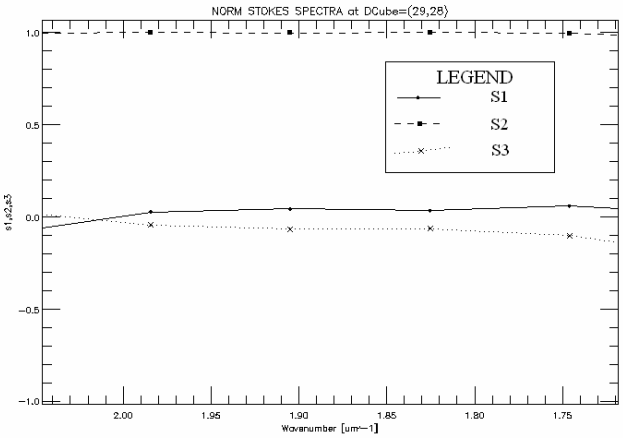

Figure 16a: normalized reconstructed Stokes spectra, 45° polarization (green)

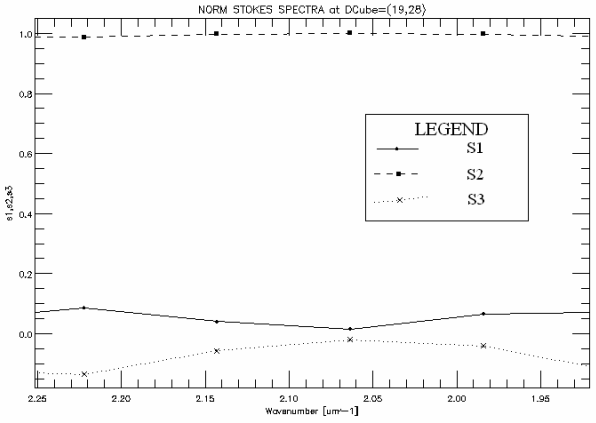

Figure 16b: normalized reconstructed Stokes spectra, 45° polarization (blue)

3. Reconstructions of uniform spatial illumination

To further test the capabilities of the CTICS instrument, polarized images were taken with uniform spatial illumination. An integrating sphere was used with a white light source that entirely filled the FOV. The panchromatic image of the reconstructed data cube is shown below in Figure 17. For each polarization state, the Stokes vector reconstructions were analyzed at three different points: the center, the upper right corner, and a point halfway between. We assumed that the field is rotationally symmetric so the three points analyzed will be representative of the other areas of the field. To avoid redundancy, only one example of the reconstructed spectra and Stokes spectra will be shown. Figure 18a and 18b show the reconstructed spectrum and Stokes spectra for horizontal polarization from a point in the upper right corner of the field. For all of the different polarization states at all points in the field, the amplitudes of the modulations are small, making them more difficult to resolve.

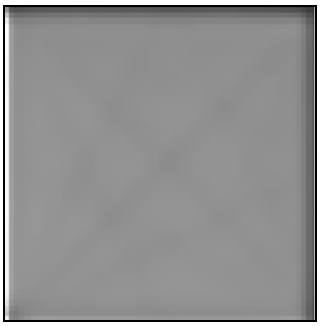

Figure 17: panchromatic image of reconstructed data cube of uniform illumination

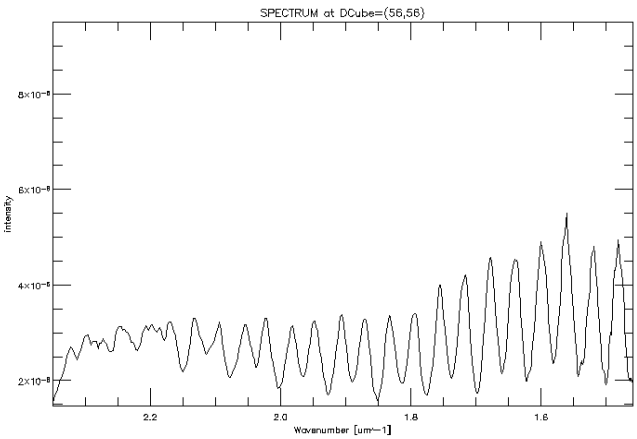

Figure 18a: reconstructed spectrum horizontal polarization (wavenumber)

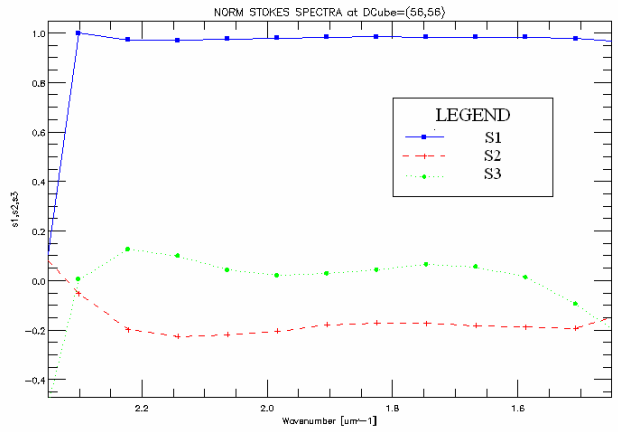

Figure 18b: reconstructed Stokes spectra horizontal polarization

ERROR ANALYSIS

In order to quantify the accuracy of the Stokes spectra reconstructions, the RMS error of each Stokes vector was calculated for all of the polarization states. The extinction ratio of the polarizer used in data collection is good enough to assume that the DoP should equal 1, meaning the light is completely polarized. The metric used to calculate the RMS error is

$$\varepsilon = \frac{1}{N}\sum_{n}\sqrt{\left(S_m - S_m^{'}\right)^2} \tag{4}$$

where N is the total number of data points and S_m represents the theoretical value of the Stokes vector being calculated at each data point (i.e. m=1 for S_1) and S_m' is the measured value of the Stokes vector at each data point. Each of the Stokes parameters was previously normalized by S_0, the DC intensity.

4. Percent error for broadband point source at edge of field

Table 1 below shows the calculated RMS percent errors for the broadband point source positioned at the edge of the instrument FOV. The percent errors at the edge of the field can be compared to percent errors from a broadband point source in the center of the field.[6] Table 2 shows the calculated RMS percent errors for a broadband point source at the center of the field.[6]

Table 1: calculated percent error in Stokes vectors from point source at edge of FOV

	S1 RMS error (%)	S2 RMS error (%)	S3 RMS error (%)
unpolarized	0.85	0.68	0.51
horizontal	0.03	1.07	0.62
vertical	0.06	1.61	0.38
45°	1.35	0.06	1.11

Table 2: calculated percent error in Stokes vectors from point source at center of FOV[6]

	S1 RMS error (%)	S2 RMS error (%)	S3 RMS error (%)
unpolarized	0.69	0.83	1.10
horizontal	0.18	1.80	1.90
vertical	0.00	1.10	0.64
45°	1.60	0.17	2.00

The percent RMS errors for the Stokes vectors do not differ much from the edge of the FOV to the center for a broadband point source. The errors are slightly better at the edge of the field than the center, especially for S_3.

5. Percent errors for green and blue LEDs

The percent RMS errors for the polarized green and blue LEDs are shown in Table 3. The RMS errors for the blue LED are larger than the errors for the green LED. Data was taken from the same image for the blue and green LEDs for each polarization, but the points were in different regions of the field. The difference in error could have to do with the quality of the data from the different spectral regions or the spatial region in the field stop. From the results above for the broadband point source at different field positions, it seems unlikely that the error between the blue and green LEDs would be caused by the field location.

Table 3: percent RMS errors calculated for each Stokes vector

BLUE RMS ERRORS

	S1 RMS error (%)	S2 RMS error (%)	S3 RMS error (%)
horizontal	0.74	7.11	3.98
vertical	0.28	3.78	2.09
45°	2.56	0.30	4.03

GREEN RMS ERRORS

	S1 RMS error (%)	S2 RMS error (%)	S3 RMS error (%)
horizontal	0.53	5.71	3.29
vertical	0.00	1.47	0.89
45°	1.77	0.15	3.61

6. Percent errors for uniform spatial illumination

Table 4 shows the percent errors for the images taken with uniform spatial illumination. Stokes vectors were analyzed at three points in the field: center, middle, and the upper right hand corner. The percentage errors are much higher for every polarization state than the errors calculated with more point-like objects. This is due to the spatial spread of the diffraction orders causing decreased contrast in the modulations. For a point-like object, the modulations of the spectrum have minimum amplitudes of about zero, whereas the modulations for a uniform spatial object have much larger minimum amplitudes. As seen in Table 4, the errors for the unpolarized, horizontal and vertical polarizations generally get smaller as we move away from the center of the field. However, 45° polarization is the opposite; the errors get larger as we move towards the edge of the FOV.

Table 4: percent RMS errors calculated for each Stokes vector with uniform spatial illumination

RMS ERRORS Unpolarized

	S1 RMS error (%)	S2 RMS error (%)	S3 RMS error (%)
center	3.50	3.10	5.29
middle	2.72	5.56	2.11
corner	0.61	1.00	1.24

RMS ERRORS Horizontal polarization

	S1 RMS error (%)	S2 RMS error (%)	S3 RMS error (%)
center	2.96	4.05	7.60
middle	1.85	6.92	4.37
corner	0.47	5.56	1.98

RMS ERRORS Vertical polarization

	S1 RMS error (%)	S2 RMS error (%)	S3 RMS error (%)
center	2.31	6.06	4.86
middle	0.49	5.12	2.32
corner	0.59	6.26	1.72

RMS ERRORS 45° polarization

	S1 RMS error (%)	S2 RMS error (%)	S3 RMS error (%)
center	5.60	0.87	3.03
middle	5.52	1.36	4.62
corner	7.15	3.62	3.05

CONCLUSION

This work presents the initial results obtained using a calibrated CTICS instrument. The goal of the CTICS is to reconstruct full spatial, spectral and Stokes polarimetric information from an object using a single focal plane array integration time with no moving parts. From this research effort, a CTICS incorporating a channeled spectropolarimeter was designed, built, and calibrated, and initial in-lab testing has begun. Reconstructions of the initial data show good agreement with theory. The polarization induced modulated spectra are shown in the reconstructions for each polarization state tested. Reconstructions of the unpolarized data show just the DC intensity with no modulations in the spectrum, as expected. Percent error was calculated for the Stokes spectra reconstructions. The error estimates from the initial data give a good starting point as we continue to improve the instrument.

REFERENCES

1. C. Vandervlugt, H. Masterson, N. Hagen, and E. Dereniak, "Reconfigurable liquid crystal dispersing element for computed tomography imaging spectrometer," in *Algorithms and Technologies for Multispectral, Hyperspectral, and Ultraspectral Imagery XIII*, S. S. Shen and P. E. Lewis, eds., *Proc. SPIE* **6565**, 65650O, 2007.
2. N. Hagen, E. L. Dereniak, and D. T. Sass, "Maximizing the resolution of a CTIS instrument," in *Imaging Spectrometry XI*, S. S. Shen and P. E. Lewis, eds., *Proc. SPIE* **6302**, 36020L, 2006.
3. N. Hagen, A. Locke, D. Sabatke, E. Dereniak, and D. Sass, "Methods and applications of snapshot spectropolarimetry," in *Polarization: Measurement, Analysis and Remote Sensing VI*, D. H. Goldstein and D. B. Chenault, eds., *Proc. SPIE* **5432**, pp. 167-174, 2004.
4. K. Oka, "Singleshot spectroscopic polarimetry using channeled spectrum," in *Advanced Materials and Devices for Sensing and Imaging*, J. Yao and Y. Ishii, eds., *Proc. SPIE* **4919**, pp. 167–175, 2002.
5. C.E. Volin, "Portable Snapshot Infrared Imaging Spectrometer," Ph.D. dissertation, University of Arizona, Tucson, AZ, 2000.
6. C. Vandervlugt, N. Hagen, R. Sampson, E. Dereniak, and G. Gerhart, "Visible Imaging Spectropolarimeter," in *Imaging Spectrometry XII*, S. S. Shen and P. E. Lewis, eds., Proc. SPIE 6661, 666104, 2007.